

MOF Composites | *Very Important Paper* **Sodium-Doped C_3N_4 /MOF Heterojunction Composites with Tunable Band Structures for Photocatalysis: Interplay between Light Harvesting and Electron Transfer**Yating Pan, Dandan Li, and Hai-Long Jiang^{*[a]}

Abstract: The search for ideal model systems to investigate the role of different parameters in heterojunction composites for enhanced photocatalysis is a high-priority target. Herein, a series of heterojunction composites, namely $Na_x-C_3N_4/Pt@UiO-66$, being composed of UiO-66 and Na-doped $g-C_3N_4$ with adjustable light absorbance and band structures, have been prepared with different Na contents, which exhibit a volcano curve towards photocatalytic H_2 production. Benefiting from the interplay of the two critical factors between light harvesting ability and electron transfer efficiency, the optimized $Na_{0.02}-C_3N_4/Pt@UiO-66$ shows excellent photocatalytic H_2 production, far surpassing its corresponding single counterparts.

Photocatalytic hydrogen production by water splitting has been regarded as a potential solution for converting solar energy into chemical energy to meet the challenge of global energy crisis.^[1] It has been recognized that the photocatalytic procedures consist of three key steps, including light harvesting (particularly, visible light), electron-hole separation and surface chemical reactions.^[2] Accordingly, various strategies and catalyst systems have been investigated to drive these processes.^[3] Amongst them, the fabrication of heterojunctions is one of the most effective strategy to overcome the drawbacks of fast charge recombination and the limited visible-light harvesting of photocatalysts.^[4] Energy level matching and effective photoexcited electron transfer are the key factors in the heterojunction formation.^[5] The classical heterojunction is formed between different semiconductor materials. In addition, different crystal phases/planes, which possess different band structures, of the same semiconductor can also create heterojunctions.^[2d,4] However, there has not yet been a systematic investi-

gation on the band structure regulation in semiconductor/semiconductor heterojunction photocatalysts to optimize the catalytic activity via systematically adjusting the light harvesting and electron transfer.^[6]


Metal-organic frameworks (MOFs),^[7] a class of crystalline porous solids constructed by metal ions or metal clusters with organic linkers, have been recognized to be promising photocatalysts for diverse reactions, including water splitting, CO_2 reduction and organic transformation based on their semiconductor-like behavior under illumination.^[8-11] The porosity and crystalline nature endow MOFs with highly dispersed active sites, short charge transfer distance and rapid pore surface reaction of charge carriers.^[12c,12c] Therefore, MOF-based materials have been widely applied for photocatalysis. Unfortunately, most MOFs suffer from limited visible-light absorption, unfavorable to their photocatalysis. To address this issue, the integration of visible-light-responsive semiconductor with them might be an effective solution.^[5,12] Behaving as an important type of semiconductor, $g-C_3N_4$ is able to harvest visible light and its light-responsive range can be adjusted by different contents of Na doping.^[6,13] The $\pi-\pi$ interaction between the triazine ring of $g-C_3N_4$ and the abundant aromatic ligands in MOFs, as well as the surface electrostatic interaction, may facilitate their close contact, heterojunction formation and electron transfer.^[5]


Bearing the above in mind, a series of heterojunction composites, $Na_x-C_3N_4/Pt@UiO-66$ (x means the molar concentration of the Na precursor solution; it denotes $g-C_3N_4/Pt@UiO-66$ when $x=0$), have been fabricated based on a representative MOF, UiO-66,^[14] and the band-tunable $Na_x-C_3N_4$ (or $g-C_3N_4$, $x=0$). Significantly, the energy level matching between the two components and the visible-light absorption in the heterojunction composites can be continuously adjusted by changing the Na contents. Along with increased Na contents, the band gap of $Na_x-C_3N_4$ becomes narrow and visible-light harvesting is enhanced, while electron transfer efficiency is more complex, which are affected by electron trap sites and driving force of electron transfer. The two critical parameters, visible-light harvesting and electron transfer, reach a balance to give optimal photocatalytic activity at a suitable Na content (Scheme 1). As a result, in the optimized $Na_{0.02}-C_3N_4/Pt@UiO-66$ composite, visible-light harvesting and electron transfer efficiency are well balanced and improved, giving rise to much enhanced photocatalytic H_2 production.

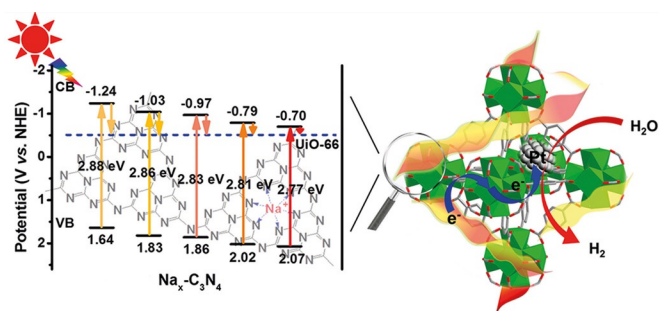
The $Na_x-C_3N_4$ were obtained by thermal polymerization and thermal oxidation etching method based on dicyandiamide

[a] Y. Pan, Dr. D. Li, Prof. Dr. H.-L. Jiang

Hefei National Laboratory for Physical Sciences at the Microscale, CAS Key Laboratory of Soft Matter Chemistry, Collaborative Innovation Center of Suzhou Nano Science and Technology, Department of Chemistry, University of Science and Technology of China, Hefei, Anhui 230026 (P. R. China)
E-mail: jianglab@ustc.edu.cn
Homepage: <http://staff.ustc.edu.cn/~jianglab/>

 Supporting information and the ORCID identification number(s) for the author(s) of this article can be found under:
<https://doi.org/10.1002/chem.201803555>

 Part of a Special Issue focusing on topics within the field of renewable energy. To view the complete issue, visit Issue 69.



Scheme 1. Schematic illustration showing the photocatalytic hydrogen production over $\text{Na}_x\text{-C}_3\text{N}_4/\text{Pt}@/\text{UiO-66}$ heterojunction composites, highlighting the tunable band structures.

and NaOH precursors.^[6a, 13b] $\text{Pt}@/\text{UiO-66}$ was prepared by adopting a double solvents approach followed by H_2 reduction, intending to the incorporation of Pt cocatalyst into the MOF.^[15] The $\text{Na}_x\text{-C}_3\text{N}_4/\text{Pt}@/\text{UiO-66}$ composites were finally fabricated by grinding $\text{Na}_x\text{-C}_3\text{N}_4$ with $\text{Pt}@/\text{UiO-66}$ and subsequent thermal treatment to enhance their interaction and improve the heterojunction formation.

The specific contents of Na in $\text{Na}_x\text{-C}_3\text{N}_4$ are decided by the inductively coupled plasma atomic emission spectrometer (ICP-AES) (Table S1). Powder X-ray diffraction patterns (PXRD) of the $\text{Na}_x\text{-C}_3\text{N}_4$ have been recorded (Figure 1A). The $\text{g-C}_3\text{N}_4$ exhibits two peaks at 13.0° and 27.4° , corresponding to its (100) and (002) crystal planes, respectively, which represent in-plane packing and interfacial stacking of $\text{g-C}_3\text{N}_4$ sheets.^[6b] For $\text{Na}_x\text{-C}_3\text{N}_4$, the peak at 13.0° shifts to lower angles along with increased Na loadings. Inversely, the peak intensity at 27.4° shifts to higher angles, indicating a larger plane spacing of the $\text{g-C}_3\text{N}_4$ triazine rings and a smaller stacking distance between $\text{g-C}_3\text{N}_4$ layers caused by Na doping. Fourier transform infrared

(FTIR) spectra of $\text{Na}_x\text{-C}_3\text{N}_4$ mainly show four bands around 810, 1200–1700, 2163 and 3000–3500 cm^{-1} (Figure 1B). The wide band region located at 1200–1700 cm^{-1} is corresponding to the aromatic C–N and C=N heterocycles stretching vibration of triazine ring framework, meanwhile, the bands at 3000–3500 cm^{-1} can be attributed to the stretching vibration of N–H groups.^[13c,d] The peak located at 810 cm^{-1} gradually weakens along with increased Na dopants, which is the characteristic breathing mode of the triazine unit. In addition, the asymmetric stretching vibration of cyano groups (–C=N) at 2162 cm^{-1} becomes relatively stronger along with increased Na loadings, demonstrating that Na has been doped into the $\text{g-C}_3\text{N}_4$ framework indeed.^[6, 13]

Theoretically, the nitride ring size (0.71 nm) of $\text{g-C}_3\text{N}_4$ is able to accommodate and coordinate with sodium ions.^[13e] X-ray photoelectron spectroscopy (XPS) results indicate that, in reference to the $\text{g-C}_3\text{N}_4$, the Na 1s XPS spectrum of $\text{Na}_{0.02}\text{-C}_3\text{N}_4$ gives a new peak at 1071.4 eV (Figure 1C), which is evidently lower than the Na–O bond at 1072.1 eV, suggesting the presence of Na–N bond.^[6] Upon the Na introduction, slight shift of binding energy is found in N 1s XPS spectra, while nothing change in the C 1s spectra can be observed (Figure S1), further supporting the formation of Na–N bond, but not Na–C bond. Therefore, the sodium ion is assumed to be fitted into the nitride cage of $\text{g-C}_3\text{N}_4$ surrounded by the heptane rings.

The absorbance edge of $\text{Na}_x\text{-C}_3\text{N}_4$ undergoes slight red shift, suggesting that the visible-light harvesting ability is gradually improved, as the content of Na increases (Figure 1D). Accordingly, the band gap energies (E_g) of $\text{Na}_x\text{-C}_3\text{N}_4$, which obtained from the Kubelka–Munk function curve transformation, change continuously from 2.88 to 2.77 eV along with increased Na loadings. On this basis, the band structures $\text{Na}_x\text{-C}_3\text{N}_4$ with different Na contents can be evaluated according to the Mott–Schottky analysis (Table S2).^[10c, 16] The bottom of conduction band (CB) in the $\text{Na}_x\text{-C}_3\text{N}_4$ decreases with the increased Na contents, inferring the lower electron-donating ability. The results unambiguously show that, light harvesting and electron transfer ability, the two critical issues in photocatalysis, can be tuned by changing Na contents in $\text{Na}_x\text{-C}_3\text{N}_4$.

The $\text{Na}_x\text{-C}_3\text{N}_4/\text{Pt}@/\text{UiO-66}$ composites have also been carefully characterized by XPS (Figure 1), PXRD and FTIR (Figure S3), in which $\text{Na}_x\text{-C}_3\text{N}_4$ and $\text{Pt}@/\text{UiO-66}$ maintain their respective structural features. In addition, the characteristic breathing mode of the triazine unit in $\text{Na}_x\text{-C}_3\text{N}_4$ (810 cm^{-1}) is still remained, revealing its structural integrity after the composite formation. Transmission electron microscopy (TEM) observation shows detailed structure of $\text{Na}_x\text{-C}_3\text{N}_4/\text{Pt}@/\text{UiO-66}$ ($\text{Na}_{0.02}\text{-C}_3\text{N}_4/\text{Pt}@/\text{UiO-66}$ as a representative), in which the Pt nanoparticles of ≈ 1.6 nm are similar to those in $\text{Pt}@/\text{UiO-66}$ (Figure 2A, 2B, S4). Both TEM and scanning electron microscope (SEM) images for $\text{Pt}@/\text{UiO-66}$ present the smooth and clean surfaces, while the sample surface is apparently rough and believed to be tightly covered by the corrugated $\text{Na}_x\text{-C}_3\text{N}_4$ layers in $\text{Na}_{0.02}\text{-C}_3\text{N}_4/\text{Pt}@/\text{UiO-66}$ (Figure 2B, S4, S5). The close contact between $\text{Pt}@/\text{UiO-66}$ and $\text{Na}_x\text{-C}_3\text{N}_4$ would greatly facilitate the formation of heterojunction. The interaction between them has been investigated by the N 1s and C 1s XPS spectra of $\text{Na}_{0.02}\text{-C}_3\text{N}_4/\text{Pt}@/\text{UiO-66}$ as a repre-

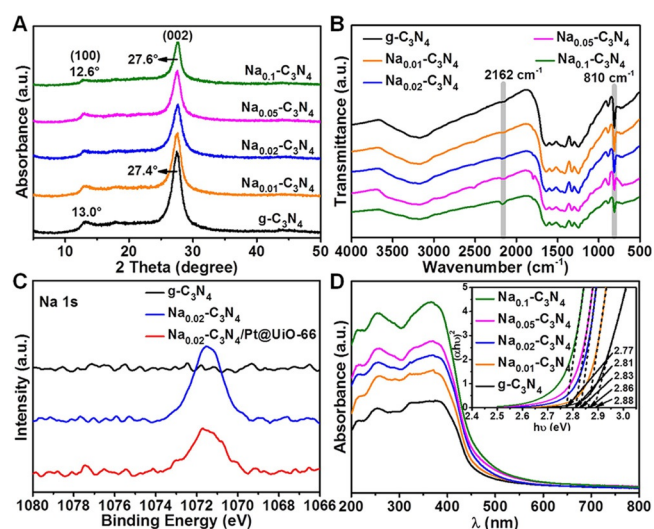


Figure 1. A) PXRD patterns, B) FTIR spectra of $\text{Na}_x\text{-C}_3\text{N}_4$, C) the Na 1s XPS spectra of $\text{g-C}_3\text{N}_4$, $\text{Na}_{0.02}\text{-C}_3\text{N}_4$ and $\text{Na}_{0.02}\text{-C}_3\text{N}_4/\text{Pt}@/\text{UiO-66}$ and D) UV/Vis absorption spectra of $\text{Na}_x\text{-C}_3\text{N}_4$. Inset: the plots of transformed Kubelka–Munk function versus the light absorption energy of $\text{Na}_x\text{-C}_3\text{N}_4$ ($x = 0, 0.01, 0.02, 0.05, \text{ and } 0.1$ m).

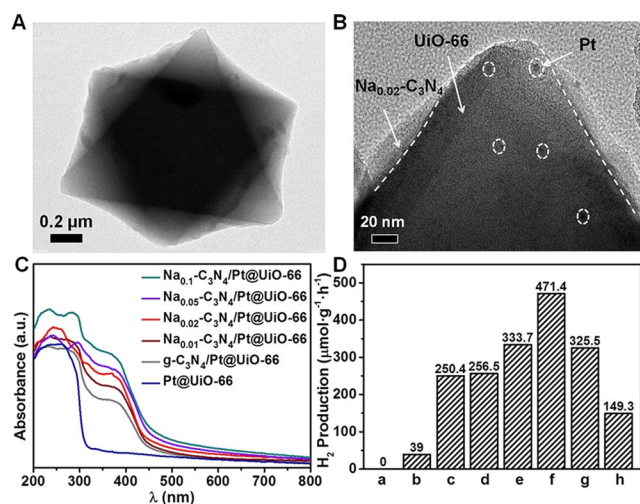


Figure 2. A) TEM image, B) enlarged TEM image of Na_{0.02}-C₃N₄/Pt@UiO-66, C) UV/Vis absorption spectra of Na_x-C₃N₄/Pt@UiO-66 and Pt@UiO-66 and D) the photocatalytic hydrogen production of a) UiO-66, b) Na_{0.02}-C₃N₄, c) physical mixture of Na_{0.02}-C₃N₄ and Pt@UiO-66 and d–h) Na_x-C₃N₄/Pt@UiO-66 ($x=0, 0.01, 0.02, 0.05, \text{ and } 0.1$ m) in MeCN/TEA/H₂O (29.5:0.5:0.15 v/v, 30 mL).

representative (Figure S1). All N 1s peaks and the C 1s peak centered at 288.3 eV (C=N-C) shift to higher binding energies, indicating the strong interaction between Na_{0.02}-C₃N₄ and Pt@UiO-66, which may be caused by π - π stacking between Na_{0.02}-C₃N₄ and Pt@UiO-66. In addition, Pt@UiO-66 is UV-light-responsive only with absorbance edge at 320 nm (Figure 2C). Upon the combination with Na_x-C₃N₄, the strong visible-light response ability has been integrated into the Na_x-C₃N₄/Pt@UiO-66 heterojunction composites. The light harvesting ability of the composites becomes stronger with the increased Na doping amounts, similar to the light absorbance trend of Na_x-C₃N₄.

With the above results, we are now in a position to investigate the photocatalytic activity. Pt@UiO-66 has no light absorbance in visible region. Therefore, no appreciable H₂ evolution was detected under visible-light irradiation. In contrast, Na_x-C₃N₄/Pt@UiO-66 composites afford considerable photocatalytic activity due to their better response in the visible-light region. Along with higher Na contents in Na_x-C₃N₄/Pt@UiO-66 ($x=0-0.02$), the composites offer improved light harvesting ability, causing enhanced visible-light photocatalytic activity. When the Na loading further increases ($x=0.02-0.1$), though the visible-light absorbance of the composites is continuously improved, unexpectedly, their activity presents gradually declined trend (Figure 2D). With the optimized Na content, the resultant Na_{0.02}-C₃N₄/Pt@UiO-66 exhibits almost 10 times of higher photocatalytic activity than single Na_{0.02}-C₃N₄ and \approx two times than that of the physical mixture of Na_{0.02}-C₃N₄ and Pt@UiO-66 (Figure 2D, S6), highlighting the enhanced activity caused by the heterojunction. The PXRD patterns for all Na_x-C₃N₄/Pt@UiO-66 catalysts after reaction demonstrate their structural stability (Figure S7). As described above, the photocatalytic activity of the Na_x-C₃N₄/Pt@UiO-66 turns out to be a volcano curve. Since this trend is not in accordance with the trend of light absorb-

ance ability (continuous enhancement along with increased Na contents), there must be other factors that simultaneously affect the activity, resulting in the best performance of Na_{0.02}-C₃N₄/Pt@UiO-66.

The photocatalytic procedure was investigated by the electron paramagnetic resonance (EPR). Upon light irradiation in the presence of TEOA as a sacrificial agent, the EPR signals of Na_x-C₃N₄/UiO-66 at $g=2.009$ and 2.030 are significantly enhanced, which might be attributed to O₂^{•-}-trapped Zr-oxo clusters (Figure S8).^[17] It is proposed that the residual O₂ molecules accept electrons from electron-trapped Zr-oxo clusters, which means the visible-light photoexcited electron transfer from Na_x-C₃N₄ to UiO-66. After the formation of heterojunction composites, the photoluminescence spectrum (PL) intensity is obviously reduced, which further suggests the efficient electron transfer (Figure S9). Based on the above information, the electron transfer efficiency might be another key factor to affect the activity.

More experiments were conducted to evaluate the relationship between electron transfer and photocatalytic activity. It is assumed that the introduction of sodium ion into g-C₃N₄ can create structural defects and lead to electron trap sites that promote the electron-hole separation according to previous reports.^[6b,10c] This is in consistent with the gradually decreased PL intensity of Na_x-C₃N₄ along with increased Na contents, which might be attributed to inhibited electron-hole recombination by the trap sites (Figure 3A, S10). The results are further supported by both transient photocurrent and electrochemical impedance spectroscopy (EIS) measurements, manifesting the faster charge separation in Na_x-C₃N₄ along with the larger x value (Figure S11, S12).^[13g]

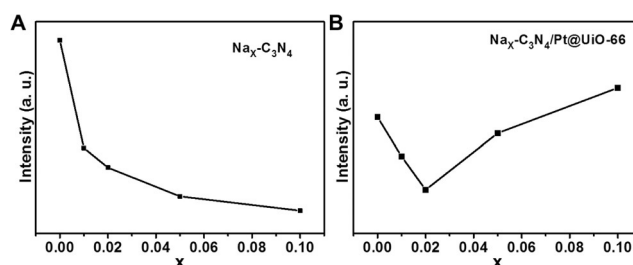


Figure 3. The photoluminescence intensity curves of A) Na_x-C₃N₄ and B) Na_x-C₃N₄/Pt@UiO-66 vs. Na contents ($x=0, 0.01, 0.02, 0.05, \text{ and } 0.1$ m).

Intuitively, the trend of electron transfer efficiency in Na_x-C₃N₄/Pt@UiO-66 heterojunction composites with the Na content change will be similar to the above Na_x-C₃N₄. However, in reference to Na_x-C₃N₄, the PL intensity of the composites gives a different order, where the lowest PL intensity is corresponding to Na_{0.02}-C₃N₄/Pt@UiO-66 rather than Na_{0.1}-C₃N₄/Pt@UiO-66 (Figure 3B, S10). This unusual phenomenon might be explained that the electron transfer in the composites is co-contributed by Na doping (giving rise to electron trap states) and energy level difference between Na_x-C₃N₄ and the MOF. As mentioned above, the electron trap sites by Na doping is favorable to the electron transfer in Na_x-C₃N₄. In addition, from

the energy diagram, the bottom of CB of all $\text{Na}_x\text{-C}_3\text{N}_4$ are more negative than that of the lowest unoccupied molecular orbital (LUMO) of UiO-66 (-0.51 V vs. NHE at pH 7.0, Figure S2, S13). A higher Na content leads to the lower CB and the smaller energy level difference relative to the lowest unoccupied molecular orbital (LUMO) of UiO-66, causing weaker driving force of electron transfer between $\text{Na}_x\text{-C}_3\text{N}_4$ and UiO-66 (Scheme 1).^[4b] Therefore, the above two factors (electron trap site and energy level difference) with positive and negative effects, respectively, to electron transfer along with increased Na contents interplay: 1) When the Na content is lower than 0.02 M, electron trap site is a major factor; 2) when the Na content is higher than 0.02 M, the trend becomes inverse and the energy level difference is a major factor. In this case, the electron transfer efficiency along with increased Na loadings presents a volcano curve, which is well supported by both photocurrent response and EIS results (Figure S11, S12). Therefore, such an electron transfer efficiency (volcano type) in combination with light harvesting ability versus the Na content in the $\text{Na}_x\text{-C}_3\text{N}_4/\text{Pt@UiO-66}$ heterojunction composites are two key factors, and they interplay to give the resultant volcano curve of their photocatalytic activity along with increased Na contents.

In summary, the $\text{Na}_x\text{-C}_3\text{N}_4/\text{Pt@UiO-66}$ heterojunction composites featuring tunable light-harvesting and band structures have been fabricated. In addition to improved light-harvesting ability, the electron transfer stemmed from electron trap sites and thermodynamic driving force (energy level difference) presents the volcano curve and gives the best efficiency at 0.02 M of Na content, along with the increased Na loadings. These two factors (light harvesting and electron transfer) interplay to afford a volcano-type activity curve of the composites versus the Na content, in which the optimized $\text{Na}_{0.02}\text{-C}_3\text{N}_4/\text{Pt@UiO-66}$ provides the best photocatalytic H_2 production rate, far surpassing any other component counterpart. This work provides an ideal model system to investigate the heterojunction composites with tunable light harvesting and band structures toward enhanced photocatalysis. The results reported herein would be informative for the further development of heterojunction photocatalysts.

Experimental Section

Preparation of $\text{Na}_x\text{-C}_3\text{N}_4$: The $\text{Na}_x\text{-C}_3\text{N}_4$ were synthesized according to the previous report with some modifications.^[6a,13c] Typically, di-cyandiamide (1 g) was dispersed into deionized water (5 mL) under stirring. Then, NaOH solution (5 mL, 0.01, 0.02, 0.05 or 0.1 M) was added. The suspension obtained was sonicated for 2 h, then heated to 100°C to evaporate water, followed by grinding at the mortar agate and annealing at 550°C for 4 h with a ramp rate of $2.3^\circ\text{Cmin}^{-1}$ and finally cooling at a rate of 1°Cmin^{-1} . The product was ground and placed in an open ceramic container heating at 500°C for 2 h with a ramp rate of 5°Cmin^{-1} . The obtained product was denoted as $\text{Na}_x\text{-C}_3\text{N}_4$, where x stands for the NaOH molar concentration. The $\text{g-C}_3\text{N}_4$ was prepared by replacing NaOH solution with de-ionized water.

Preparation of UiO-66: Typically, ZrCl_4 (20 mg), BDC (14.25 mg) and DMF (10 mL) were ultrasonically dissolved in a 20 mL Pyrex

vial. The mixture was heated in 120°C oven for 24 h. After cooling down to room temperature, the precipitate was recovered by centrifugation and washed with DMF and methanol for several times, and finally dried at 60°C under vacuum overnight.

Preparation of Pt@UiO-66: The Pt@UiO-66 was prepared via a double solvents approach.^[14] Typically, a certain amount of UiO-66 was activated at 120°C for 2 h. The activated UiO-66 (100 mg) was suspended in hexane (20 mL) and the mixture was sonicated for around 60 min until they became homogeneous. After being stirred for a certain time, H_2PtCl_6 (14.3 μL) solution with desired concentrations ($\text{Pt}/\text{UiO-66} = 1/100$ wt %) was added dropwise during constant vigorous stirring. Subsequently, the resultant solution was continuously stirred for 4 h. The solid was collected by centrifugation and dried in 85°C and Pt was finally reduced by H_2/Ar mixed gas (H_2 , 20% v/v) at 200°C .

Preparation of $\text{Na}_x\text{-C}_3\text{N}_4/\text{Pt@UiO-66}$: Typically, $\text{Na}_x\text{-C}_3\text{N}_4$ (5 mg) and Pt@UiO-66 (10 mg) were mixed and ground for 30 min in the mortar agate using a pestle, then thermally treated at 350°C for 2 h in N_2 atmosphere in a tubular furnace to produce the $\text{Na}_x\text{-C}_3\text{N}_4/\text{Pt@UiO-66}$ heterojunction composites. The same batch of Pt@UiO-66 was used in this procedure.

Photocatalytic experiments: Typically, photocatalyst (3 mg) was dispersed in acetonitrile (29.5 mL) and deionized water (0.15 mL) with triethylamine (TEA, 0.5 mL) as a sacrificial reagent in an optical reaction vessel. Then, the suspension was stirred and purged with nitrogen for 15 min to remove air. The reaction vessel with reaction solution was fixed, and irradiated by the 300 W Xe lamp equipped with a UV cut-off filter (>380 nm). Hydrogen gas was measured by gas chromatography (Shimadzu GC-2014) using a thermal conductivity detector (TCD).

Photoelectrochemical measurements: Photoelectrochemical measurements were performed on a CHI 760E electrochemical work station (Chenhua Instrument, Shanghai, China) in a standard three-electrode system with the photocatalyst-coated ITO as the working electrode, Pt plate as the counter electrode, and Ag/AgCl as a reference electrode. A 300 W Xenon lamp with a UV cut-off filter (>380 nm) was used as light source. A 0.1 M Na_2SO_4 solution was used as electrolyte. The catalyst (2 mg) was dispersed into a solution containing Nafion (10 μL) and ethanol (3 mL), and the working electrodes were prepared by dropping the suspension (200 μL) onto the surface of an ITO plate. The working electrodes were dried at room temperature, and the photoresponsive signals of the samples were measured under chopped light with a bias potential of $+0.5$ V.

Electrochemical impedance spectroscopy and Mott-Schottky

plot measurements: The electrochemical impedance spectroscopy was performed on the Zahner Zennium electrochemical workstation in a standard three-electrode system with the photocatalyst-coated glassy carbon ($\Phi = 3$ cm) as the working electrode, Pt plate as counter electrode, and an Ag/AgCl as a reference electrode. A 0.1 M Na_2SO_4 aqueous solution was used as the electrolyte. The samples (2 mg) was dispersed into a solution of 5 wt % Nafion (10 μL) and ethanol (3 mL), and the working electrode was prepared by dropping the suspension (30 μL) onto the surface of the glassy carbon electrode. The working electrode was dried, and then EIS measurement was performed with a bias potential of -1.65 V for $\text{Na}_x\text{-C}_3\text{N}_4$ and -1.7 V for $\text{Na}_x\text{-C}_3\text{N}_4/\text{Pt@UiO-66}$ in the dark. Mott-Schottky plots were measured by changing the frequencies of Ag/AgCl reference electrode at 500, 1000, and 1500 Hz, respectively.

Acknowledgements

This work was supported by the NSFC (21725101, 21673213, 21701160 and 21521001), the National Research Fund for Fundamental Key Project (2014CB931803) and the Fundamental Research Funds for the Central Universities (WK2060030029).

Conflict of interest

The authors declare no conflict of interest.

Keywords: electron transfer · g-C₃N₄ · light harvesting · metal-organic frameworks · photocatalysis

- [1] a) J. Ran, J. Zhang, J. Yu, M. Jaroniec, S. Z. Qiao, *Chem. Soc. Rev.* **2014**, *43*, 7787–7812; b) H. Tong, S. Ouyang, Y. Bi, N. Umezawa, M. Oshikiri, J. Ye, *Adv. Mater.* **2012**, *24*, 229–251; c) N. S. Lewis, D. G. Nocera, *Proc. Natl. Acad. Sci. USA* **2006**, *103*, 15729–15735.
- [2] a) A. Kudo, Y. Miseki, *Chem. Soc. Rev.* **2009**, *38*, 253–278; b) Y. Yang, S. W. Niu, D. D. Han, T. Y. Liu, G. M. Wang, Y. Li, *Adv. Energy Mater.* **2017**, *7*, 1700555; c) T. Zhang, W. Lin, *Chem. Soc. Rev.* **2014**, *43*, 5982–5993; d) J. X. Low, J. G. Yu, M. Jaroniec, S. Wageh, A. A. Al-Ghamdi, *Adv. Mater.* **2017**, *29*, 1601694.
- [3] a) Z. Zou, J. Ye, K. Sayama, H. Arakawa, *Nature* **2001**, *414*, 625–627; b) X. Chen, S. Shen, L. Guo, S. S. Mao, *Chem. Rev.* **2010**, *110*, 6503–6570; c) J. Liu, Y. Liu, N. Liu, Y. Han, X. Zhang, H. Huang, Y. Lifshitz, S. T. Lee, J. Zhong, Z. Kang, *Science* **2015**, *347*, 970–974; d) D. Z. Zee, T. Chantarojsiri, J. R. Long, C. J. Chang, *Acc. Chem. Res.* **2015**, *48*, 2027–2036; e) H. Liu, C. Y. Xu, D. D. Li, H.-L. Jiang, *Angew. Chem. Int. Ed.* **2018**, *57*, 5379–5383; *Angew. Chem.* **2018**, *130*, 5477–5481; f) M. S. Zhu, Z. C. Sun, M. Fujitsuka, T. Majima, *Angew. Chem. Int. Ed.* **2018**, *57*, 2160–2164; *Angew. Chem.* **2018**, *130*, 2182–2186; g) Z. Jiang, W. Wan, H. Li, S. Yuan, H. Zhao, P. K. Wong, *Adv. Mater.* **2018**, *30*, 1706108.
- [4] a) H. Wang, L. Zhang, Z. Chen, J. Hu, S. Li, Z. Wang, J. Liu, X. Wang, *Chem. Soc. Rev.* **2014**, *43*, 5234–5244; b) Y. Ma, X. Wang, Y. Jia, X. Chen, H. Han, C. Li, *Chem. Rev.* **2014**, *114*, 9987–10043.
- [5] a) R. Wang, L. Gu, J. Zhou, X. Liu, F. Teng, C. Li, Y. Shen, Y. Yuan, *Adv. Mater. Interfaces* **2015**, *2*, 1500037; b) L. Shi, T. Wang, H. B. Zhang, K. Chang, J. Ye, *Adv. Funct. Mater.* **2015**, *25*, 5360–5367.
- [6] a) J. Zhang, S. Hu, Y. Wang, *RSC Adv.* **2014**, *4*, 62912–62919; b) H. Yu, R. Shi, Y. Zhao, T. Bian, Y. Zhao, C. Zhou, G. I. N. Waterhouse, L. Z. Wu, C. H. Tung, T. Zhang, *Adv. Mater.* **2017**, *29*, 1605148.
- [7] a) H.-C. Zhou, S. Kitagawa, *Chem. Soc. Rev.* **2014**, *43*, 5415–5418; b) B. Li, H. M. Wen, Y. J. Cui, W. Zhou, G. D. Qian, B. L. Chen, *Adv. Mater.* **2016**, *28*, 8819–8860; c) L. Jiao, Y. Wang, H.-L. Jiang, Q. Xu, *Adv. Mater.* **2018**, *30*, 201703663; d) G. Cai, W. Zhang, L. Jiao, S.-H. Yu, H.-L. Jiang, *Chem* **2017**, *2*, 791–802; e) M.-S. Yao, X.-J. Lv, Z.-H. Fu, W.-H. Li, W.-H. Deng, G.-D. Wu, G. Xu, *Angew. Chem. Int. Ed.* **2017**, *56*, 16510–16514; *Angew. Chem.* **2017**, *129*, 16737–16741.
- [8] a) M. Alvaro, E. Carbonell, B. Ferrer, F. X. L. I. Xamena, H. Garcia, *Chem. Eur. J.* **2007**, *13*, 5106–5112; b) Z. L. Wu, C. H. Wang, B. Zhao, J. Dong, F. Lu, W. H. Wang, W. C. Wang, G. J. Wu, J. Z. Cui, P. Cheng, *Angew. Chem. Int. Ed.* **2016**, *55*, 4938–4942; *Angew. Chem.* **2016**, *128*, 5022–5026; c) Z. Li, J.-D. Xiao, H.-L. Jiang, *ACS Catal.* **2016**, *6*, 5359–5365; d) R.-W. Huang, Y.-S. Wei, X.-Y. Dong, X.-H. Wu, C.-X. Du, S.-Q. Zang, T. C. W. Mak, *Nat. Chem.* **2017**, *9*, 689–697; e) X. Y. Dong, M. Zhang, R. B. Pei, Q. Wang, D. H. Wei, S. Q. Zang, Y. T. Fan, T. C. W. Mak, *Angew. Chem. Int. Ed.* **2016**, *55*, 2073–2077; *Angew. Chem.* **2016**, *128*, 2113–2117.
- [9] a) T. Zhou, Y. Du, A. Borgna, J. Hong, Y. Wang, J. Han, W. Zhang, R. Xu, *Energy Environ. Sci.* **2013**, *6*, 3229–3234; b) S. Pullen, H. Fei, A. Orthaber, S. M. Cohen, S. Ott, *J. Am. Chem. Soc.* **2013**, *135*, 16997–17003; c) M. Wen, K. Mori, T. Kamegawa, H. Yamashita, *Chem. Commun.* **2014**, *50*, 11645–11648; d) J. D. Xiao, Q. C. Shang, Y. J. Xiong, Q. Zhang, Y. Luo, S. H. Yu, H.-L. Jiang, *Angew. Chem. Int. Ed.* **2016**, *55*, 9389–9393; *Angew. Chem.* **2016**, *128*, 9535–9539; e) D. Kim, D. R. Whang, S. Y. Park, *J. Am. Chem. Soc.* **2016**, *138*, 8698–8701; f) S. Z. Yang, B. Pattengale, E. L. Kovrigin, J. Huang, *ACS Energy Lett.* **2017**, *2*, 75–80; g) Y. An, Y. Liu, P. An, J. Dong, B. Xu, Y. Dai, X. Qin, X. Zhang, M.-H. Whangbo, B. Huang, *Angew. Chem. Int. Ed.* **2017**, *56*, 3036–3040; *Angew. Chem.* **2017**, *129*, 3082–3086; h) J. D. Xiao, L. L. Han, J. Luo, S. H. Yu, H.-L. Jiang, *Angew. Chem. Int. Ed.* **2018**, *57*, 1103–1107.
- [10] a) C. Wang, K. E. deKrafft, W. Lin, *J. Am. Chem. Soc.* **2012**, *134*, 7211–7214; b) Y. Fu, D. Sun, Y. Chen, R. Huang, Z. Ding, X. Fu, Z. Li, *Angew. Chem. Int. Ed.* **2012**, *51*, 3364–3367; *Angew. Chem.* **2012**, *124*, 3420–3423; c) H.-Q. Xu, J. Hu, D. Wang, Z. Li, Q. Zhang, Y. Luo, S.-H. Yu, H.-L. Jiang, *J. Am. Chem. Soc.* **2015**, *137*, 13440–13443; d) Y. Wang, N. Y. Huang, J. Q. Shen, P. Q. Liao, X. M. Chen, J. P. Zhang, *J. Am. Chem. Soc.* **2018**, *140*, 38–41.
- [11] a) Y. Zhang, J. Guo, L. Shi, Y. F. Zhu, K. Hou, Y. L. Zheng, Z. Y. Tang, *Sci Adv.* **2017**, *3*, e1701162; b) X. Deng, Z. Li, H. Garcia, *Chem. Eur. J.* **2017**, *23*, 11189–11209.
- [12] a) J. He, J. Wang, Y. Chen, J. Zhang, D. Duan, Y. Wang, Z. Yan, *Chem. Commun.* **2014**, *50*, 7063–7066; b) Y.-P. Yuan, L.-S. Yin, S.-W. Cao, G.-S. Xu, C.-H. Li, C. Xue, *Appl. Catal. B* **2015**, *168–169*, 572–576; c) D. Li, S.-H. Yu, H.-L. Jiang, *Adv. Mater.* **2018**, *30*, 1707377.
- [13] a) T. Xiong, W. Cen, Y. Zhang, F. Dong, *ACS Catal.* **2016**, *6*, 2462–2472; b) P. Niu, L. Zhang, G. Liu, H.-M. Cheng, *Adv. Funct. Mater.* **2012**, *22*, 4763–4770; c) A. Thomas, A. Fischer, F. Goettmann, M. Antonietti, J. O. Muller, R. Schlogl, J. M. Carlsson, *J. Mater. Chem.* **2008**, *18*, 4893–4908; d) X. Wang, K. Maeda, A. Thomas, K. Takanebe, G. Xin, J. M. Carlsson, K. Domen, M. Antonietti, *Nat. Mater.* **2009**, *8*, 76–80; e) X. G. Ma, Y. H. Lv, J. Xu, Y. F. Liu, R. Q. Zhang, Y. F. Zhu, *J. Phys. Chem. C* **2012**, *116*, 23485–23493; f) W. J. Ong, L. L. Tan, Y. H. Ng, S. T. Yong, S. P. Chai, *Chem. Rev.* **2016**, *116*, 7159–7329; g) W. Che, W. Cheng, T. Yao, F. Tang, W. Liu, H. Su, Y. Huang, Q. Liu, J. Liu, F. Hu, Z. Pan, Z. Sun, S. Wei, *J. Am. Chem. Soc.* **2017**, *139*, 3021–3026.
- [14] J. H. Cavka, S. Jakobsen, U. Olsbye, N. Guillou, C. Lamberti, S. Bordiga, K. P. Lillerud, *J. Am. Chem. Soc.* **2008**, *130*, 13850–13851.
- [15] a) A. Aijaz, A. Karkamkar, Y. J. Choi, N. Tsumori, E. Rönnebro, T. Autrey, H. Shioyama, Q. Xu, *J. Am. Chem. Soc.* **2012**, *134*, 13926–13929; b) Y. Z. Chen, Y. X. Zhou, H. W. Wang, J. L. Lu, T. Uchida, Q. Xu, S. H. Yu, H.-L. Jiang, *ACS Catal.* **2015**, *5*, 2062–2069.
- [16] K. Maeda, K. Sekizawa, O. Ishitani, *Chem. Commun.* **2013**, *49*, 10127–10129.
- [17] J. Long, S. Wang, Z. Ding, S. Wang, Y. Zhou, L. Huang, X. Wang, *Chem. Commun.* **2012**, *48*, 11656–11658.

Manuscript received: July 11, 2018

Accepted manuscript online: August 28, 2018

Version of record online: October 2, 2018